

## Article

# Preparation and Thermal Conductivity of Epoxy Resin/Graphene-Fe<sub>3</sub>O<sub>4</sub> Composites

Zhong Wu<sup>1</sup>, Jingyun Chen<sup>1</sup>, Qifeng Li<sup>1</sup>, Da-Hai Xia<sup>1</sup> , Yida Deng<sup>1</sup>, Yiwen Zhang<sup>1</sup> and Zhenbo Qin<sup>1,2,\*</sup>

<sup>1</sup> Tianjin Key Laboratory of Composite and Functional Materials, School of Material Science and Engineering, Tianjin University, Tianjin 300072, China; wuzhong2319@163.com (Z.W.); jingyun19961229@163.com (J.C.); qifengli@tju.edu.cn (Q.L.); dahaixia@tju.edu.cn (D.-H.X.); yida.deng@tju.edu.cn (Y.D.); ywzsci@tju.edu.cn (Y.Z.)

<sup>2</sup> Key Laboratory of Advanced Ceramics and Machining Technology (Ministry of Education), Tianjin University, Tianjin 300072, China

\* Correspondence: qinzhb@tju.edu.cn

**Abstract:** By modifying the bonding of graphene (GR) and Fe<sub>3</sub>O<sub>4</sub>, a stable structure of GR-Fe<sub>3</sub>O<sub>4</sub>, namely magnetic GR, was obtained. Under the induction of a magnetic field, it can be orientated in an epoxy resin (EP) matrix, thus preparing EP/GR-Fe<sub>3</sub>O<sub>4</sub> composites. The effects of the content of GR and the degree of orientation on the thermal conductivity of the composites were investigated, and the most suitable Fe<sub>3</sub>O<sub>4</sub> load on GR was obtained. When the mass ratio of GR and Fe<sub>3</sub>O<sub>4</sub> was 2:1, the thermal conductivity could be increased by 54.8% compared with that of pure EP. Meanwhile, EP/GR-Fe<sub>3</sub>O<sub>4</sub> composites had a better thermal stability, dynamic thermomechanical properties, and excellent electrical insulation properties, which can meet the requirements of electronic packaging materials.

**Keywords:** magnetic GR; EP/GR-Fe<sub>3</sub>O<sub>4</sub> composites; orientation; thermal conductivity



**Citation:** Wu, Z.; Chen, J.; Li, Q.; Xia, D.-H.; Deng, Y.; Zhang, Y.; Qin, Z.

Preparation and Thermal Conductivity of Epoxy Resin/Graphene-Fe<sub>3</sub>O<sub>4</sub> Composites. *Materials* **2021**, *14*, 2013. <https://doi.org/10.3390/ma14082013>

Academic Editor: Vlassios Likodimos

Received: 15 March 2021

Accepted: 14 April 2021

Published: 16 April 2021

**Publisher's Note:** MDPI stays neutral with regard to jurisdictional claims in published maps and institutional affiliations.



**Copyright:** © 2021 by the authors. Licensee MDPI, Basel, Switzerland. This article is an open access article distributed under the terms and conditions of the Creative Commons Attribution (CC BY) license (<https://creativecommons.org/licenses/by/4.0/>).

## 1. Introduction

Epoxy resin (EP) sealing materials are widely used in the field of electronic packaging due to their excellent electrical insulation and mechanical properties. However, the heat-conducting property of EP is very poor, and the intrinsic thermal conductivity is only 0.18 W/mK [1]. With the development of miniaturization of electronic equipment, the phenomenon of heat generation becomes more and more serious, which will greatly shorten the service life of the equipment [2]. Therefore, improving the thermal conductivity of EP is an efficient technical means to solve this problem. At present, several conductive particles (SiC [3,4], Al<sub>2</sub>O<sub>3</sub> [5–7], AlN [8–11], and SiO<sub>2</sub> [12]) are used to improve the thermal conductivity of EP. However, the improvement effect is not obvious. To effectively improve the heat dissipation rate of EP, the suggestion of constructing a heat conduction channel by adding graphene (GR) to an EP matrix has been proposed. Because of the extremely high thermal conductivity of GR in the in-plane direction, it is crucial to ensure the directional distribution of GR in an EP matrix. There are many methods to achieve directional distribution of GR in an matrix, including the flow shear induction method [13], solution pouring method [14], vacuum dead-end microporous filtration method [15], vacuum pumping filtration method [16], and the magnetic field induction method [17]. The magnetic field induction method refers to the directional arrangement of magnetic GR in a magnetic field, which is widely used because of its safety and simple operation. Therefore, the preparation of magnetic GR is a goal that researchers have been exploring. Zhu successfully loaded magnetic nanoparticles on the surface of GR via chemical co-precipitation [18]. Ma prepared GR loaded with Fe<sub>3</sub>O<sub>4</sub> nanoparticles using a decomposition reduction method [19]. Guo used polyelectrolyte coating technology to coat Fe<sub>3</sub>O<sub>4</sub> nanoparticles on the surface of GR [20]. Although magnetic particles can be loaded on the surface of GR using different methods, this structure is not sufficiently stable.

In this paper, magnetic GR with a stable structure was obtained using a chemical bonding method. The directional distribution of GR in an EP matrix was achieved under the induction of a magnetic field. Based on the high thermal conductivity of GR in the in-plane direction, an excellent thermal conductivity of EP/GR-Fe<sub>3</sub>O<sub>4</sub> composites was realized.

## 2. Materials and Methods

### 2.1. Materials

Graphene nanosheets were purchased from Nanjing Xianfeng Nanotechnology Co., Ltd., Nanjing, China. NH<sub>2</sub>C<sub>3</sub>H<sub>6</sub>Si(OC<sub>2</sub>H<sub>5</sub>)<sub>3</sub> (KH550) and C<sub>9</sub>H<sub>20</sub>O<sub>5</sub>Si (KH560), used as the silane coupling agent with the amino group (NH<sub>2</sub>) and epoxy group, respectively, were purchased from Aladdin Chemistry Co., Tianjin, China. FeCl<sub>3</sub>·6H<sub>2</sub>O and FeCl<sub>2</sub>·4H<sub>2</sub>O were provided by Tianjin Yuanli Chemical Co., Ltd., Tianjin, China. Bisphenol-A liquid epoxy resin (E51), phenolic amine epoxy curing agent (T31), 2,4,6-Tris (dimethylamino methyl) phenol curing accelerator (DMP-30) and epoxy resin defoamer were purchased from Nantong Xingchen Synthetic Material Co., Tianjin, China. Concentrated hydrochloric acid (HCl), sodium hydroxide (NaOH) and ethanol were purchased from Tianjin Yuanli Chemical Co., Ltd., Tianjin, China.

### 2.2. Preparation

Firstly, GR (0.3 g) was dispersed in ethanol (60 mL), then KH550 (3 mL) and HCl (1 mL) were added. The mixed solution was stirred in an oil bath at 55 °C for 5 h to obtain GR-NH<sub>2</sub> after suction filtration and ultrasonic dispersion. FeCl<sub>3</sub>·6H<sub>2</sub>O (2.0 g) and FeCl<sub>2</sub>·4H<sub>2</sub>O (0.74 g) were dissolved in deionized water (20 mL). An appropriate amount of NaOH was added to make the pH value of the solution within the range of 10–11, and the mixed solution was stirred in an oil bath at 55 °C for 2 h [21]. Then, the intermediate products obtained by filtering the above solution were added to a mixed solution of ethanol (30 mL), KH560 (1 mL) and HCl (1 mL), and stirred in an oil bath at 55 °C for 5 h. After filtration, the Fe<sub>3</sub>O<sub>4</sub>-epoxy group was obtained. Finally, GR-NH<sub>2</sub> and Fe<sub>3</sub>O<sub>4</sub>-epoxy (mass ratios are 8:1, 4:1, 2:1, respectively) were added into ethanol (60 mL) and stirred in an oil bath at 60 °C for 10 h. The mixed solution was filtered to obtain magnetic GR.

E51 (8 g), T31 (2 g), DMP-30 (0.16 g) and epoxy resin defoamer (0.08 g) were added to the polytetrafluoroethylene (PTFE) mold. A certain amount of magnetic GR (the specific content is shown in Table 1) was added to the EP mixture, and the magnetic GR was evenly dispersed in the EP mixture through stirring. The mold containing a mixture of EP and magnetic GR was placed in a uniform magnetic field and stood for 24 h until the mixture was cured [22]. As described above, magnetic GRs with mass ratios of GR to Fe<sub>3</sub>O<sub>4</sub> of 8:1, 4:1, and 2:1 were prepared, numbered a, b, and c. When the mass fraction of GR in the EP was maintained as 0.034 wt.%, 0.067 wt.%, 0.100 wt.%, and 0.134 wt.%, the corresponding addition amount of magnetic GR (a, b, c) in the EP is shown in Table 1.

### 2.3. Characterization

The morphology of samples was characterized by scanning electron microscopy (SEM, JSM, 7800 F, Shishima, Tokyo, Japan) and transmission electron microscope (TEM, JEM, 2100 F, Shishima, Tokyo, Japan), and the elements were determined by the energy dispersive spectroscopy (EDS, AMETEXK EDAX, Shishima, Tokyo, Japan). The crystal structure of materials was determined by X-ray diffraction (XRD, D8 ADVANCE, Shishima, Tokyo, Japan) with Cu K $\alpha$  radiation. The microstructure of the magnetic-particle was determined by Fourier transform infrared spectrometer (FTIR, Nicolet iS10, Waltham, MA, USA). The thermal conductivity was measured by a thermal constant analyzer (TPS2500S, Hot Disk, Uppsala, Sweden). Dynamic thermomechanical analysis (DTMA) of the EP and EP/GR-Fe<sub>3</sub>O<sub>4</sub> composites were determined by TA Instrument Thermal Mechanical Analyzer (TMA, Q800, New Castle, DE, USA). Thermo-gravimetric analysis (TGA) was carried out with a synchronous thermal analyzer (STA449, Selbu, Germany). The volume

resistivity of EP and its composites were measured with an ultrahigh electric resistivity meter (ZC36, Shanghai, China). The test voltages for the samples were 250 V and 1000 V.

**Table 1.** The mass fraction of magnetic graphene (GR) in epoxy resin (EP).

Mass Fraction of GR in EP (wt.%)	Mass Fraction of Magnetic GR in EP (wt.%)
0.034	0.038 (a)
	0.040 (b)
	0.050 (c)
0.067	0.075 (a)
	0.080 (b)
	0.100 (c)
0.100	0.113 (a)
	0.125 (b)
	0.150 (c)
0.134	0.150 (a)
	0.167 (b)
	0.200 (c)

(a) Magnetic GR with mass ratio of GR to  $\text{Fe}_3\text{O}_4$  of 8:1, (b) Magnetic GR with mass ratio of GR to  $\text{Fe}_3\text{O}_4$  of 4:1, (c) Magnetic GR with mass ratio of GR to  $\text{Fe}_3\text{O}_4$  of 2:1.

### 3. Results and Discussion

#### 3.1. Material Characterization

$\text{Fe}_3\text{O}_4$  is a black crystal with magnetism, commonly known as magnetic iron oxide, which is a complex oxide. The ferromagnetic material prepared has typical  $\text{Fe}_3\text{O}_4$  diffraction peaks. As shown in Figure 1, the positions at  $30.1^\circ$ ,  $35.4^\circ$ ,  $43.1^\circ$ ,  $56.9^\circ$ , and  $62.5^\circ$  correspond to the diffraction peaks (220), (311), (400), (511), (440) of  $\text{Fe}_3\text{O}_4$ , respectively [21]. GR has a characteristic peak of (002) at  $26.5^\circ$ . Additionally, the prepared magnetic GR was also characterized by XRD, and it was found that the characteristic peaks of GR and  $\text{Fe}_3\text{O}_4$  existed at the same time, indicating that GR- $\text{Fe}_3\text{O}_4$  was successfully prepared. To determine whether  $\text{Fe}_3\text{O}_4$  and GR was chemically bonded, FTIR characterization was performed.

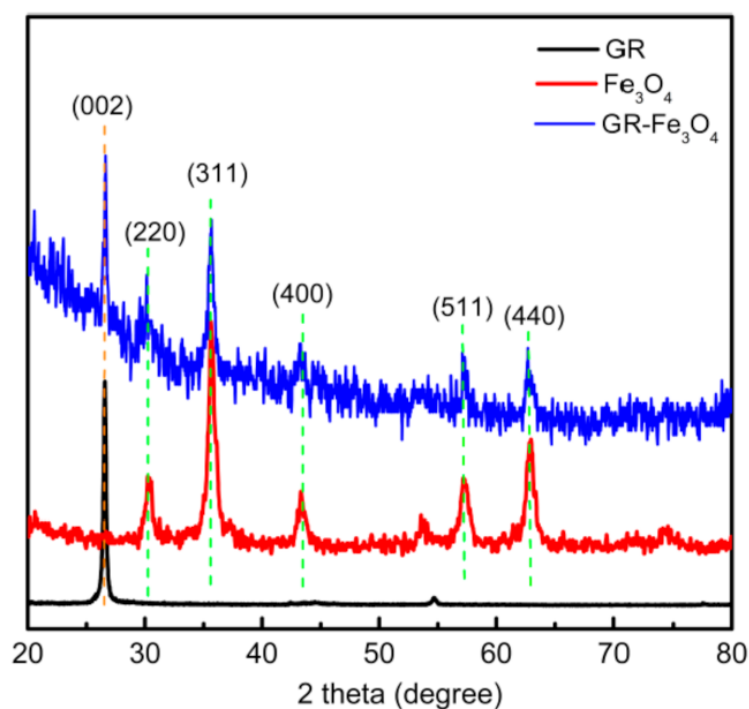


**Figure 1.** XRD patterns of GR,  $\text{Fe}_3\text{O}_4$  and magnetic GR (GR- $\text{Fe}_3\text{O}_4$ ).

Figure 2 shows the corresponding preparation schematic diagram. Steps (1), (2), and (3) are the preparation principles of GR-NH<sub>2</sub>, Fe<sub>3</sub>O<sub>4</sub>-epoxy, and magnetic GR, respectively. Step (1): the KH550 with NH<sub>2</sub> reacts with the hydroxyl groups of the GR, so that the GR is loaded with NH<sub>2</sub>. Step (2): the Fe<sub>3</sub>O<sub>4</sub> with hydroxyl groups reacts with KH560 with epoxy groups to make Fe<sub>3</sub>O<sub>4</sub> have epoxy groups. Step (3): through the reaction between the NH<sub>2</sub> and epoxy groups, the magnetic particles Fe<sub>3</sub>O<sub>4</sub> are attached to the GR. Figure 3 shows the FTIR spectra of GR-NH<sub>2</sub>, Fe<sub>3</sub>O<sub>4</sub>-epoxy and GR-Fe<sub>3</sub>O<sub>4</sub>. In the FTIR spectrum, the stretching vibration peak of Si-O is at 1043 cm<sup>-1</sup> [23]. The absorption peak at 3326 cm<sup>-1</sup> corresponds to the stretching vibration peak of NH<sub>2</sub>. The antisymmetric stretching vibration peaks of methylene on KH550 and KH560 are at 2920 cm<sup>-1</sup> and 2850 cm<sup>-1</sup> [24]. The characteristic peak of Fe-O is at 580 cm<sup>-1</sup> [25–28], and the characteristic peak of epoxy group C-O is at 890 cm<sup>-1</sup> [29]. As shown in Figure 3, stretching vibration peaks of Si-O and NH<sub>2</sub> appears after the reaction of GR and KH550, indicating that GR-NH<sub>2</sub> is successfully prepared. After Fe<sub>3</sub>O<sub>4</sub> reacts with KH560, the characteristic peak of epoxy group C-O appears, as shown in Figure 3, indicating the successful preparation of Fe<sub>3</sub>O<sub>4</sub>-epoxy. When the Fe<sub>3</sub>O<sub>4</sub>-epoxy reacts with the GR-NH<sub>2</sub>, the absorption peak around 3326 cm<sup>-1</sup> becomes wider, and the characteristic peak of the epoxy group C-O at 890 cm<sup>-1</sup> disappears, indicating the successful preparation of magnetic GR.

Figure 4 shows the SEM morphology of GR, Fe<sub>3</sub>O<sub>4</sub>, GR-Fe<sub>3</sub>O<sub>4</sub>, and EDS of GR-Fe<sub>3</sub>O<sub>4</sub>. The surface of GR has an obvious fold structure, as shown in Figure 4a. Figure 4b shows the SEM morphology of Fe<sub>3</sub>O<sub>4</sub>. Since the SEM resolution is lower than TEM, it is impossible to determine whether it is a single Fe<sub>3</sub>O<sub>4</sub> particle. There are many small particles attached to the GR, as shown in Figure 4c. EDS characterization test was performed on the particles on magnetic GR, which is depicted in Figure 4d. Element peaks associated with iron and oxygen are detected, indicating that Fe<sub>3</sub>O<sub>4</sub> particles loaded on the GR sheet.

The prepared magnetic GR was further observed by TEM. As shown in Figure 5, Fe<sub>3</sub>O<sub>4</sub> particles are evenly distributed on the GR flakes. The ones with lattice fringes at high magnification are Fe<sub>3</sub>O<sub>4</sub>, and the diameter of a single crystal grain is in the range of 15–20 nm. The electron diffraction patterns are (220), (311), (400), (511), and (440), respectively, indicating that the chemical bonding of GR and Fe<sub>3</sub>O<sub>4</sub> did not change the crystal structure of the Fe<sub>3</sub>O<sub>4</sub> particles.

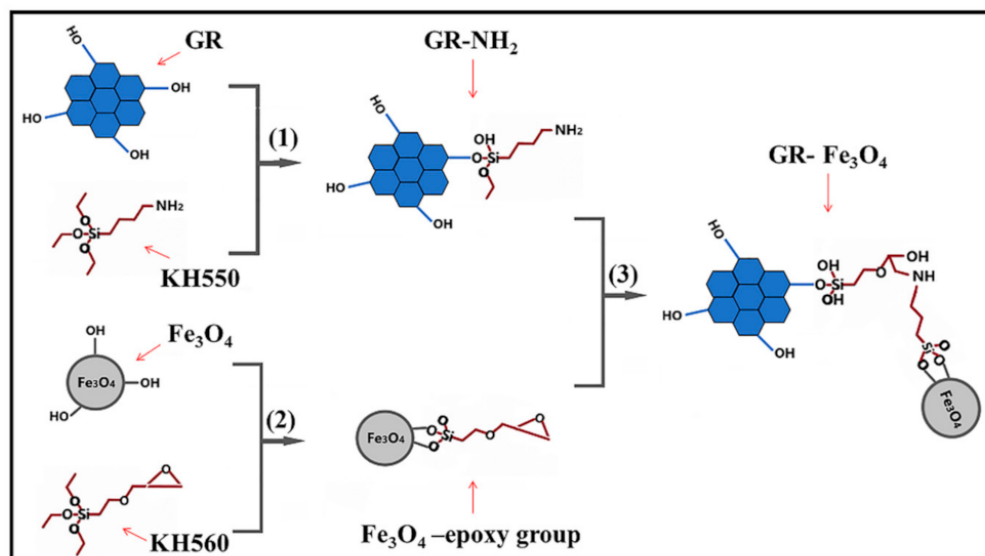


Figure 2. Schematic diagram of magnetic GR preparation.

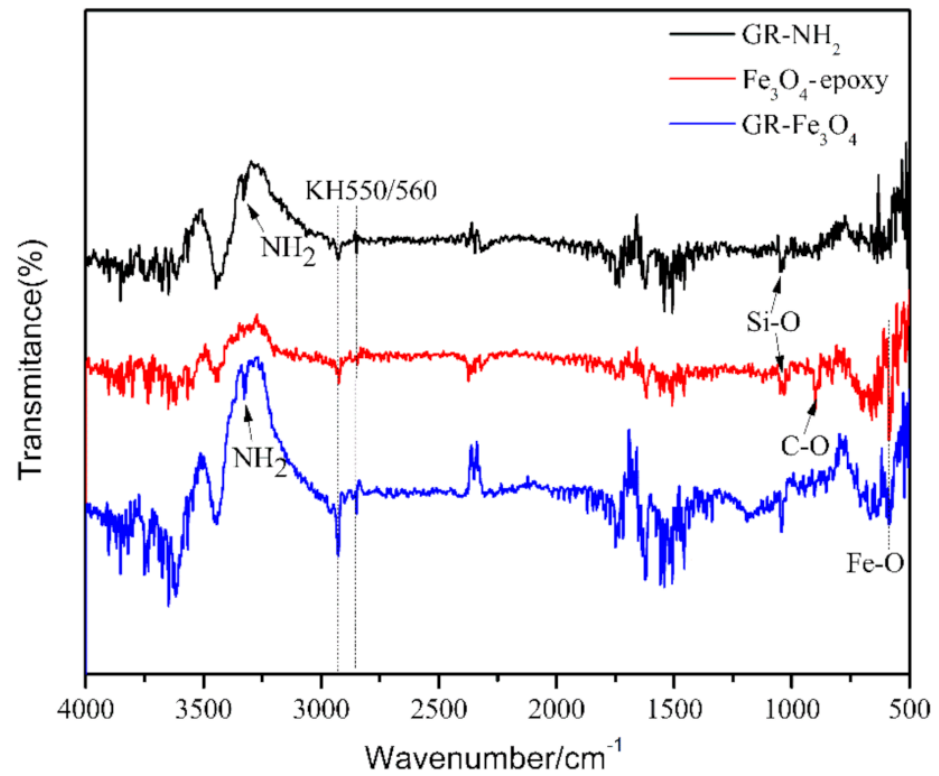


Figure 3. FTIR spectra of GR-NH<sub>2</sub>, Fe<sub>3</sub>O<sub>4</sub>-epoxy and GR-Fe<sub>3</sub>O<sub>4</sub>.

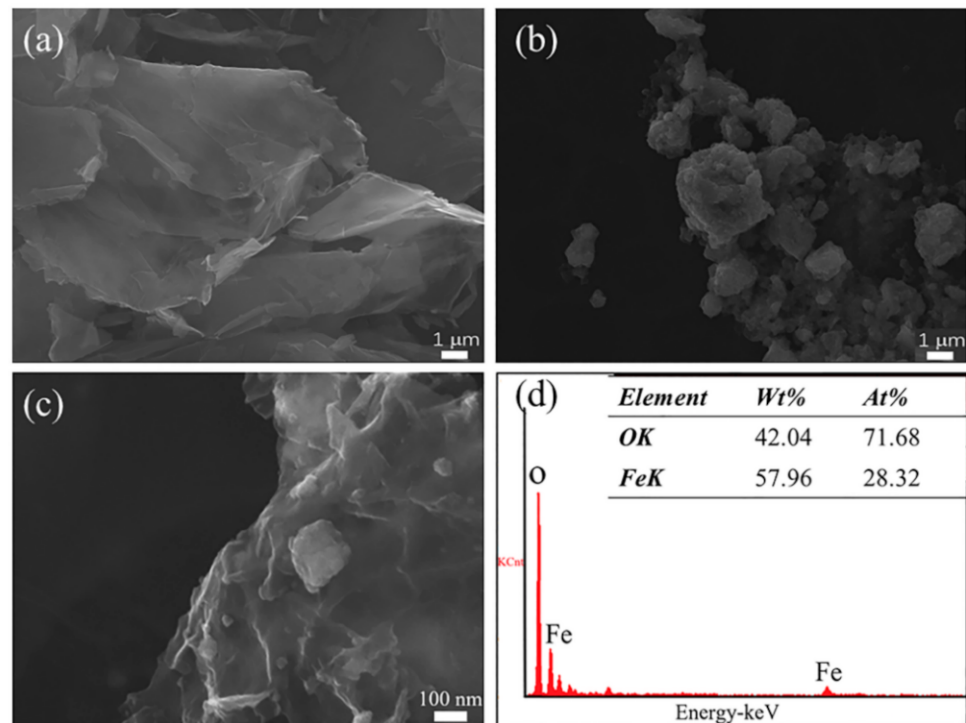
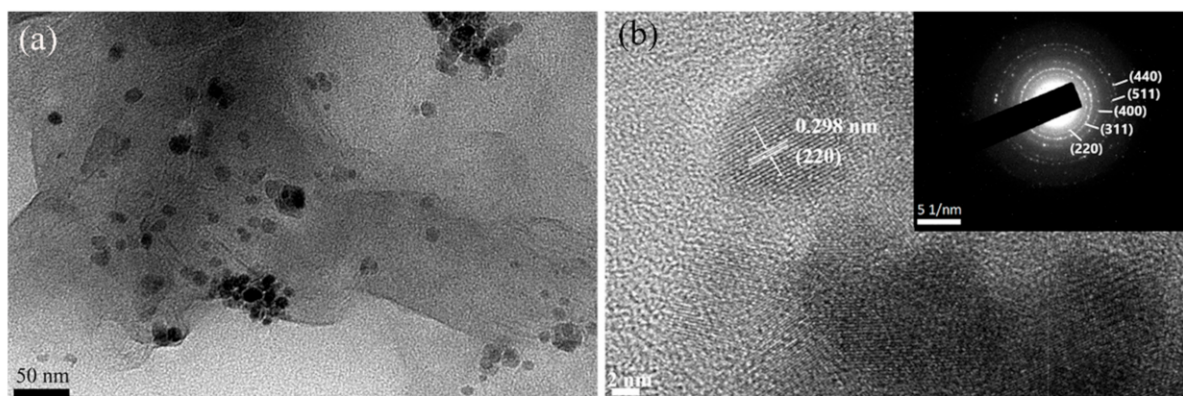
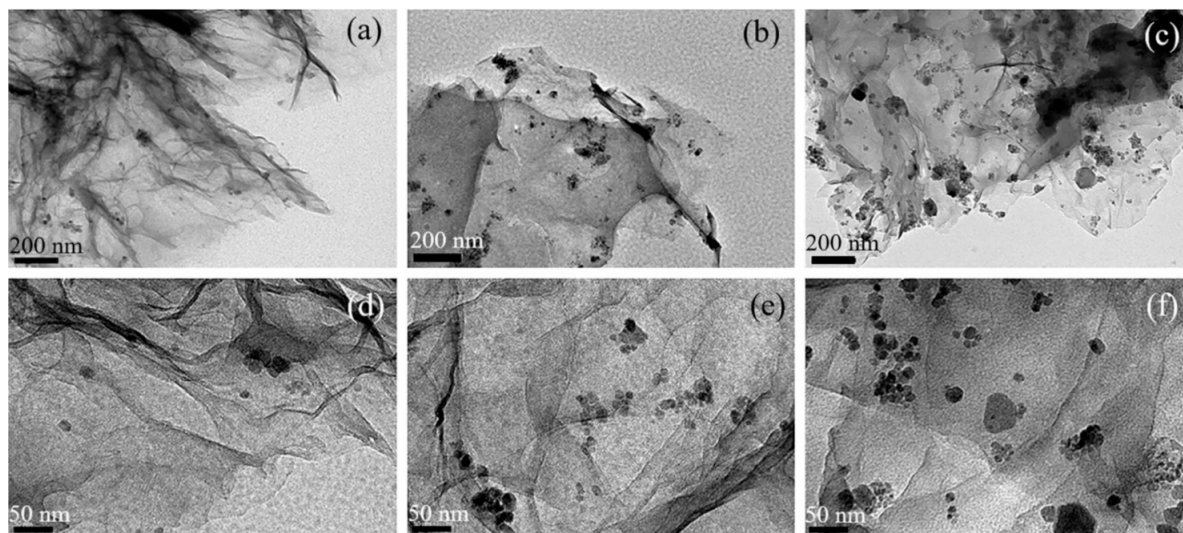


Figure 4. SEM images of (a) GR, (b) Fe<sub>3</sub>O<sub>4</sub>, (c) GR-Fe<sub>3</sub>O<sub>4</sub>; (d) the EDS of GR-Fe<sub>3</sub>O<sub>4</sub>.



**Figure 5.** TEM image (a) and electron diffraction pattern (b) of GR-Fe<sub>3</sub>O<sub>4</sub>.

The mass ratios of GR and Fe<sub>3</sub>O<sub>4</sub> are 8:1, 4:1, 2:1, respectively. According to the different loading content of Fe<sub>3</sub>O<sub>4</sub> on GR, the orientation degree of GR in the magnetic field is also different. It is expected that the more loading of Fe<sub>3</sub>O<sub>4</sub> content, the more horizontal and oriented the distribution of GR in EP will be, which will significantly improve the thermal conductivity. TEM characterization of GR with different loadings of Fe<sub>3</sub>O<sub>4</sub> is shown in Figure 6. The macro morphology observed at 15k magnification (Figure 6a–c) indicates more Fe<sub>3</sub>O<sub>4</sub> loaded on GR with an increase in the mass ratio of Fe<sub>3</sub>O<sub>4</sub>: GR. However, from the observation at 50 k magnification (Figure 6d–f), it is found that Fe<sub>3</sub>O<sub>4</sub> has the best dispersibility without agglomeration when the mass ratio of GR: Fe<sub>3</sub>O<sub>4</sub> is 8:1. As the loading content of Fe<sub>3</sub>O<sub>4</sub> increases, Fe<sub>3</sub>O<sub>4</sub> particles begin to agglomerate on GR, but it is not obvious.



**Figure 6.** TEM images of GR-Fe<sub>3</sub>O<sub>4</sub> under different mass ratios, the mass ratios of GR: Fe<sub>3</sub>O<sub>4</sub> are 8:1 (a,d), 4: 1 (b,e), 2:1 (c,f).

### 3.2. Thermal Properties and Electrical Insulation of Composites

As shown in Figure 7, when Fe<sub>3</sub>O<sub>4</sub> is loaded on the GR, under the induction of the magnetic field, Fe<sub>3</sub>O<sub>4</sub> pulls the GR to spread along the direction parallel to the magnetic field, so that the magnetic GR can be directionally arranged in the EP matrix. The thermal conductivity of pure EP is 0.1810 W/mK, while the thermal conductivity of Fe<sub>3</sub>O<sub>4</sub> doped EP is 0.1811 W/mK, indicating that Fe<sub>3</sub>O<sub>4</sub> does not affect the thermal conductivity of EP. The specific thermal conductivity data have been listed in Table 2. In this experiment, when the content of GR was 0.134 wt.%, the thermal conductivity of composites reached 0.2801 W/mK, which was 54.8% higher than that of pure EP, that is, the thermal conductivity of the composites was about 1.55 times that of pure EP. In related studies, the content of

GR in the composites was very large, generally more than 1 wt.%. For example, adding 10 wt.% GR in EP could improve the thermal conductivity to 1.53 W/mK [30], increasing the thermal conductivity by 8.5 times. However, the content of GR in EP was 74.6 times higher than that in this study. Moreover, the high GR content would also bring a series of problems, such as increase in cost, degradation of electrical insulation performance, and so on. Considering that the EP composite are mainly used in electronic packaging, it is necessary to add the GR as little as possible to ensure its electrical insulation.

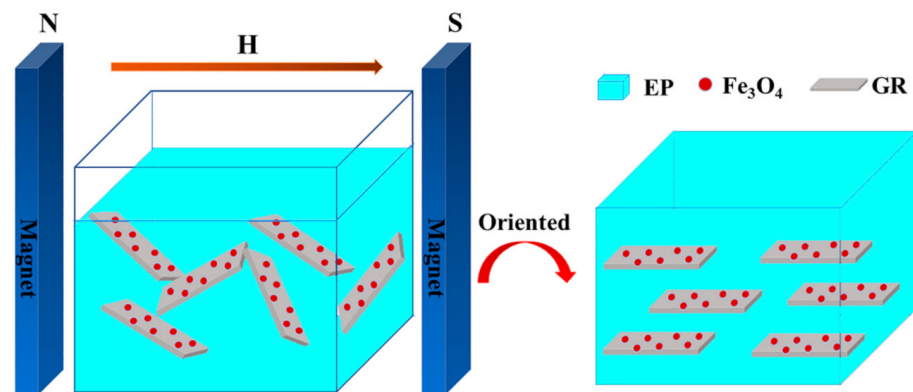


Figure 7. Schematic diagram of magnetic GR orientation under the induction of the magnetic field.

Table 2. Thermal conductivity (TC) of pure EP and EP/GR-Fe<sub>3</sub>O<sub>4</sub> composites.

The Mass Fraction of GR in EP(wt.%)	TC (W/mK)				
	Only GR	GR: Fe <sub>3</sub> O <sub>4</sub> /8:1	GR: Fe <sub>3</sub> O <sub>4</sub> /4:1	GR: Fe <sub>3</sub> O <sub>4</sub> /2:1	
0.034	0.1895 (±0.0003)	0.1902 (±0.0001)	0.1905 (±0.0004)	0.2101 (±0.0002)	
0.067	0.2058 (±0.0004)	0.2083 (±0.0004)	0.2106 (±0.0002)	0.2308 (±0.0003)	
0.100	0.2078 (±0.0004)	0.2108 (±0.0005)	0.2200 (±0.0003)	0.2666 (±0.0002)	
0.134	0.2106 (±0.0003)	0.2134 (±0.0002)	0.2259 (±0.0003)	0.2801 (±0.0004)	

As shown in Figure 8, on the premise of the same degree of GR orientation, that is, the mass ratio of GR and Fe<sub>3</sub>O<sub>4</sub> remains unchanged, the thermal conductivity increases gradually with the increase of GR content. This can be inferred from the fact that smaller content of GR tend to be wrapped by the EP and isolated from each other. With the increase of GR content, the heat transfer pathway is formed in the EP and the thermal conductivity increases.

When the mass ratio of GR to Fe<sub>3</sub>O<sub>4</sub> is 8:1 and 4:1, the content of Fe<sub>3</sub>O<sub>4</sub> is so small that GR cannot be arranged in a regular way, which results in a slight increase in thermal conductivity. When the mass ratio is 2:1, the thermal conductivity increases significantly. Therefore, it can be concluded that when the relative content of Fe<sub>3</sub>O<sub>4</sub> in magnetic GR is small, the degree of directional arrangement of magnetic GR is low and it is difficult to obtain a high thermal conductivity. Once the mass ratio reaches 2:1, the GR is arranged regularly by the rotation of Fe<sub>3</sub>O<sub>4</sub>, and its high in-plane thermal conductivity can be fully utilized. Therefore, the thermal conductivity of the composites significantly improved. Next, the dynamic thermodynamic properties, thermal stability and electrical insulation of EP and composites (when the mass ratio of GR to Fe<sub>3</sub>O<sub>4</sub> is 2:1) are studied.

The loss tangent (Tan  $\delta$ ) is an important parameter in the dynamic thermomechanical properties, which is sensitive to all molecular motions in the polymer, and the temperature corresponding to its peak can be used as the glass transition temperature (T<sub>g</sub>) of the composites [31]. Figure 9 shows the relationship of Tan  $\delta$  for EP and its composites as a function with temperature. It can be seen from the peak shift of the curves that the T<sub>g</sub> of the composites are higher than that of pure EP, and the T<sub>g</sub> gradually increases with the

increase of GR content. This is attributed to the restraint of magnetic GR on the segmental motion of epoxy near the organic/inorganic interface [32], resulting in better dynamic thermomechanical properties for composites than pure EP.

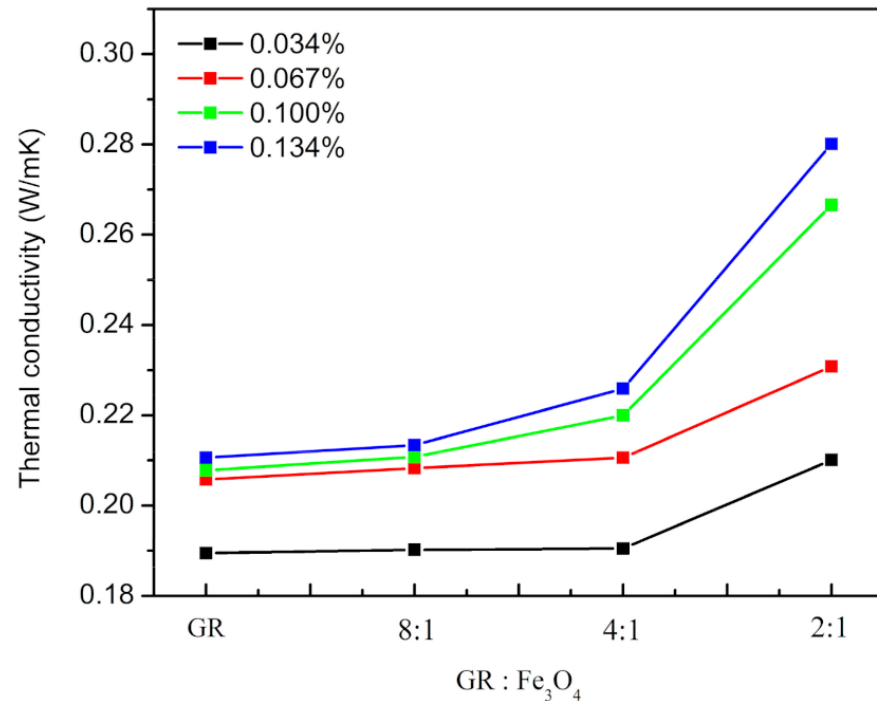


Figure 8. Thermal conductivity of EP/GR-Fe<sub>3</sub>O<sub>4</sub> composites.

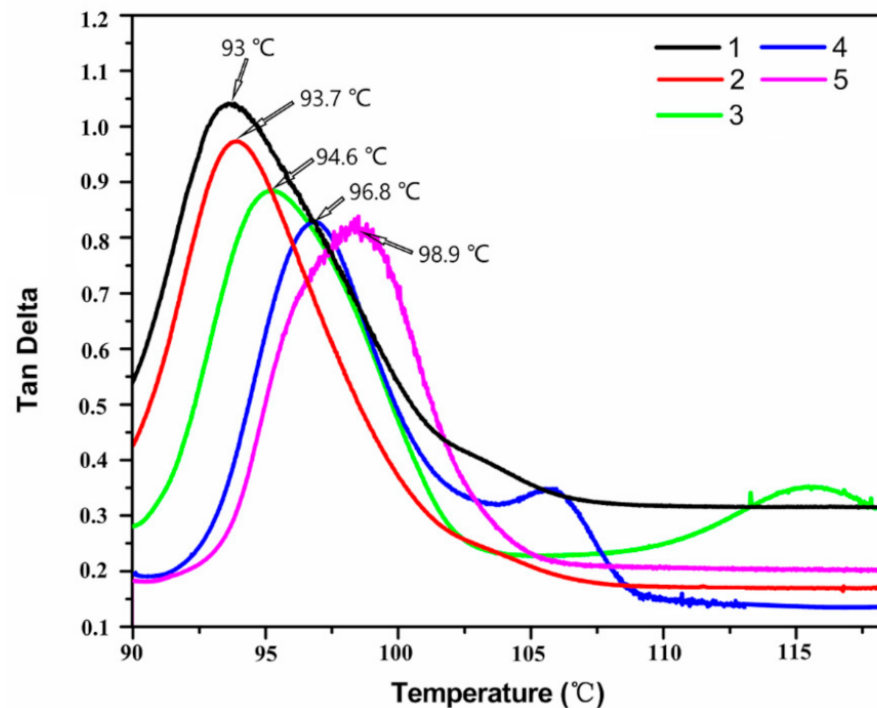
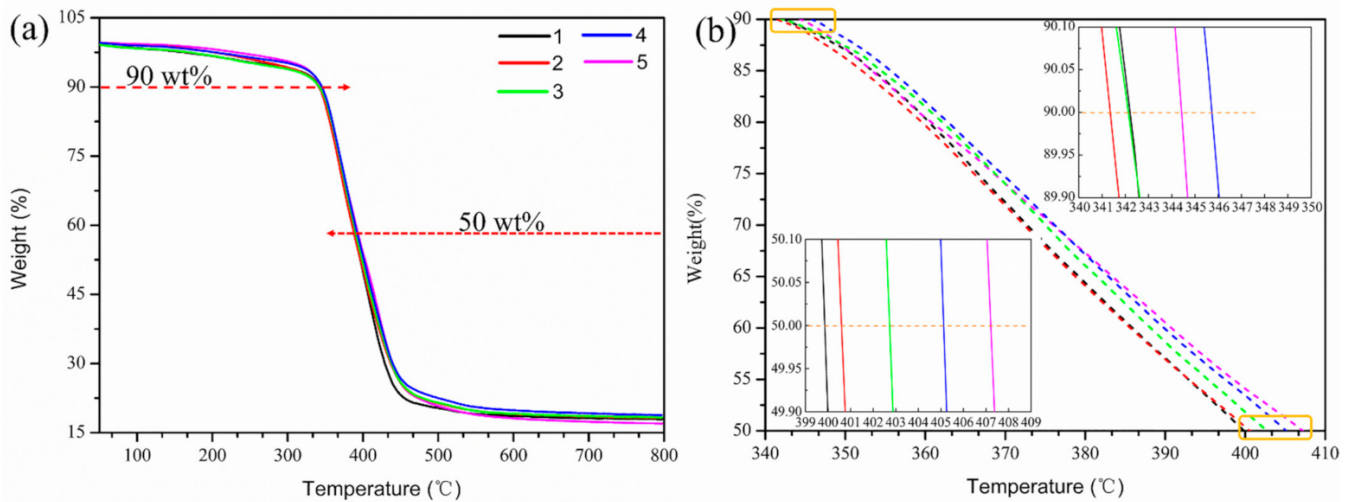


Figure 9. Dynamic thermomechanical analysis spectra of composites as a function of temperature with different magnetic GR contents. Curves 1–5 indicate that the mass fraction of magnetic GR in EP is 0.00%, 0.05%, 0.10%, 0.15%, and 0.20%, respectively.

Thermal stability of the pure EP and EP/GR-Fe<sub>3</sub>O<sub>4</sub> composites was studied by TGA. Figure 10a shows the TGA of pure EP and EP/GR-Fe<sub>3</sub>O<sub>4</sub> composites with different mass fractions of magnetic GR. It can be seen that all composites show similar thermal decomposition curves as pure EP, indicating that the content of magnetic GR does not affect the original thermal decomposition mechanism of the EP matrix [8]. Magnifying the curves between 90% and 50% weight (Figure 10b), the curves of EP/GR-Fe<sub>3</sub>O<sub>4</sub> composites decrease more slowly than that of EP. As shown in Table 3, the temperature for 10% weight loss ( $T_{10\%}$ ) and 50% weight loss ( $T_{50\%}$ ) were found that  $T_{10\%}$  of EP and EP/GR-Fe<sub>3</sub>O<sub>4</sub> are similar (the maximum difference is 3.2 °C), while  $T_{50\%}$  have a great difference (the maximum difference is 8.4 °C) between them. Compared with pure EP, the addition of magnetic GR delayed the thermal decomposition process of EP. On the one hand, GR pieces effectively restrict the thermal movement of epoxy chain segments during combustion. On the other hand, GR pieces have a high thermal capacity and thermal conductivity. The synergistic effect of the two factors delays the thermal degradation of composites, making its thermal stability better than that of pure EP [33,34].



**Figure 10.** TGA curves of pure EP and EP/GR-Fe<sub>3</sub>O<sub>4</sub> composites. Curves 1–5 indicate that the mass fraction of magnetic GR in EP is 0.00%, 0.05%, 0.10%, 0.15%, and 0.20%, respectively. (a) Overview of TGA curves; (b) magnified curves between 90 wt.% and 50 wt.%).

**Table 3.** Thermal properties of pure EP and EP/GR-Fe<sub>3</sub>O<sub>4</sub> composites.

The Mass Fraction of GR-Fe <sub>3</sub> O <sub>4</sub> in EP (wt.%)	T <sub>g</sub> (°C)	T <sub>10%</sub> (°C)	T <sub>50%</sub> (°C)
0	93.0	342.4	399.2
0.05	93.7	341.6	400.8
0.10	94.6	342.0	402.8
0.15	96.8	345.6	405.6
0.20	98.9	344.4	407.6

As for thermally conductive composites, the electrical insulation property is also a key factor in electronic packaging. Materials with high electrical insulation can ensure the safety and stability of electronic components [34]. Figure 11 shows the volume resistivity of EP and EP/GR-Fe<sub>3</sub>O<sub>4</sub> composites as a function of magnetic GR content at 250 V. The volume resistivity of the composites has little difference compared with that of pure EP, which is kept at the same order of magnitude ( $\times 10^{16} \Omega \cdot \text{cm}$ ) as that of pure EP. Moreover, none of the composites showed dielectric breakdown at the highest voltage (1000 V). Therefore, the thermal conductivity of the composites is improved on the premise of ensuring electrical insulation.

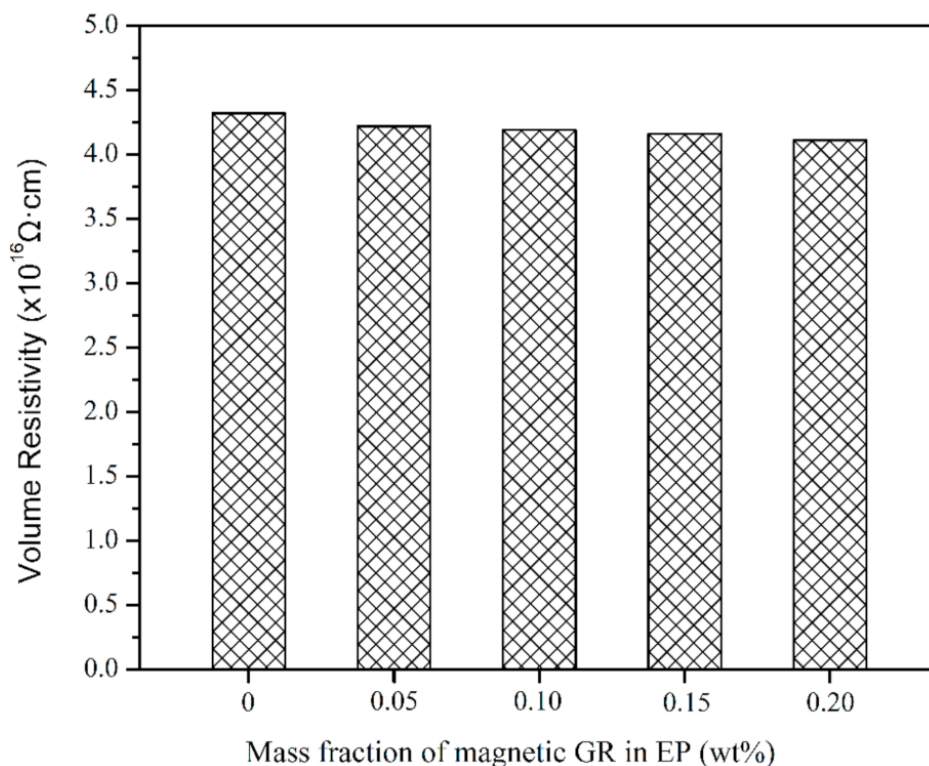


**Figure 11.** Volume resistivity of EP and EP/GR-Fe<sub>3</sub>O<sub>4</sub> composites.

#### 4. Conclusions

Using the chemical bonding method, GR and Fe<sub>3</sub>O<sub>4</sub> were modified with functional groups, and the magnetic GR was obtained by stably loading Fe<sub>3</sub>O<sub>4</sub> particles on GR sheets. The thermal properties of EP and EP/GR-Fe<sub>3</sub>O<sub>4</sub> composites were further studied. At a constant mass ratio of GR: Fe<sub>3</sub>O<sub>4</sub>, the thermal conductivity increases gradually with the increase of GR content. When the amount of Fe<sub>3</sub>O<sub>4</sub> loaded on GR is not sufficient, the orientation distribution of magnetic GR is relatively low, which results in a slight increase in thermal conductivity. When the mass ratio of GR to Fe<sub>3</sub>O<sub>4</sub> reaches 2:1, the degree of GR orientation is significantly improved, and its high in-plane thermal conductivity can be fully utilized, resulting in the significant improvement of thermal conductivity. The dynamic thermomechanical properties and thermal stability of the EP/GR-Fe<sub>3</sub>O<sub>4</sub> composites under this mass ratio are better than pure EP. Moreover, the addition of GR did not reduce the electrical insulation evidently of this composite.

**Author Contributions:** Conceptualization, Z.W. and Z.Q.; methodology, J.C.; software, J.C. and Z.W.; validation, Z.W.; formal analysis, Z.Q.; investigation, Q.L. and J.C.; resources, D.-H.X. and Y.D.; data curation, Y.Z.; writing—original draft preparation, J.C.; writing—review and editing, Z.W.; visualization, Q.L. and Y.Z.; supervision, Z.W.; project administration, Z.Q. and Y.D.; funding acquisition, Z.W. All authors have read and agreed to the published version of the manuscript.

**Funding:** This research was funded by the National Key Research and Development Program of China (2018YFB0703500) and the National Natural Science Foundation of China (No. 51971155 and No. 52001226).

**Institutional Review Board Statement:** Not applicable.

**Informed Consent Statement:** Not applicable.

**Data Availability Statement:** The data presented in this study are available upon request from the corresponding author.

**Conflicts of Interest:** The authors declare no conflict of interest.

## References

1. Xu, S.; Liu, H.; Li, Q.; Mu, Q.; Wen, H. Influence of magnetic alignment and layered structure of BN&Fe/EP on thermal conducting performance. *J. Mater. Chem. C* **2016**, *4*, 872–878. [[CrossRef](#)]
2. Kim, J.; Ma, B.; Lee, K. Comparison of effect of epoxy and silicone adhesive on the lifetime of plastic LED package. *Electron. Mater. Lett.* **2013**, *9*, 429–432. [[CrossRef](#)]
3. Zhou, T.; Wang, X.; Mingyuan, G.U.; Liu, X. Study of the thermal conduction mechanism of nano-SiC/DGEBA/EMI-2,4 composites. *Polymer* **2008**, *49*, 4666–4672. [[CrossRef](#)]
4. Li, Y.; Huang, X.; Hu, Z.; Jiang, P.; Li, S.; Tanaka, T. Large Dielectric Constant and High Thermal Conductivity in Poly(vinylidene fluoride)/Barium Titanate/Silicon Carbide Three-Phase Nanocomposites. *ACS Appl. Mater. Interfaces* **2011**, *3*, 4396–4403. [[CrossRef](#)]
5. Zhou, W.; Qi, S.; Tu, C.; Zhao, H.; Wang, C.; Kou, J. Effect of the particle size of Al<sub>2</sub>O<sub>3</sub> on the properties of filled heat-conductive silicone rubber. *J. Appl. Polym. Sci.* **2007**, *104*, 1312–1318. [[CrossRef](#)]
6. Zhang, S.; Ke, Y.; Cao, X.; Ma, Y.; Wang, F. Effect of Al<sub>2</sub>O<sub>3</sub> fibers on the thermal conductivity and mechanical properties of high density polyethylene with the absence and presence of compatibilizer. *J. Appl. Polym. Sci.* **2012**, *124*, 4874–4881. [[CrossRef](#)]
7. Heo, Y.; Im, H.; Kim, J.; Kim, J. The influence of Al(OH)<sub>3</sub>-coated graphene oxide on improved thermal conductivity and maintained electrical resistivity of Al<sub>2</sub>O<sub>3</sub>/epoxy composites. *J. Nanoparticle Res.* **2012**, *14*. [[CrossRef](#)]
8. Qian, R.; Yu, J.; Xie, L.; Li, Y.; Jiang, P. Efficient thermal properties enhancement to hyperbranched aromatic polyamide grafted aluminum nitride in epoxy composites. *Polym. Adv. Technol.* **2013**, *24*, 348–356. [[CrossRef](#)]
9. Zhou, Y.; Wang, H.; Wang, L.; Yu, K.; Lin, Z.; He, L.; Bai, Y. Fabrication and characterization of aluminum nitride polymer matrix composites with high thermal conductivity and low dielectric constant for electronic packaging. *Mater. Sci. Eng. B-Adv. Funct. Solid-State Mater.* **2012**, *177*, 892–896. [[CrossRef](#)]
10. Yu, H.; Li, L.; Kido, T.; Xi, G.; Xu, G.; Guo, F. Thermal and insulating properties of epoxy/aluminum nitride composites used for thermal interface material. *J. Appl. Polym. Sci.* **2012**, *124*, 669–677. [[CrossRef](#)]
11. Choi, S.; Im, H.; Kim, J. The thermal conductivity of embedded nano-aluminum nitride-doped multi-walled carbon nanotubes in epoxy composites containing micro-aluminum nitride particles. *Nanotechnology* **2012**, *23*. [[CrossRef](#)]
12. Zeng, J.; Fu, R.; Shen, Y.; He, H.; Song, X. High Thermal Conductive Epoxy Molding Compound with Thermal Conductive Pathway. *J. Appl. Polym. Sci.* **2009**, *113*, 2117–2125. [[CrossRef](#)]
13. Qiu, F.; Hao, Y.; Li, X.; Wang, B.; Wang, M. Functionalized graphene sheets filled isotactic polypropylene nanocomposites. *Compos. Part B-Eng.* **2015**, *71*, 175–183. [[CrossRef](#)]
14. Zhao, W.; Kong, J.; Liu, H.; Zhuang, Q.; Gu, J.; Guo, Z. Ultra-high thermally conductive and rapid heat responsive poly(benzobisoxazole) nanocomposites with self-aligned graphene. *Nanoscale* **2016**, *8*, 19984–19993. [[CrossRef](#)]
15. Lian, G.; Tuan, C.-C.; Li, L.; Jiao, S.; Wang, Q.; Moon, K.-S.; Cui, D.; Wong, C.-P. Vertically Aligned and Interconnected Graphene Networks for High Thermal Conductivity of Epoxy Composites with Ultralow Loading. *Chem. Mater.* **2016**, *28*, 6096–6104. [[CrossRef](#)]
16. Zhang, Y.-F.; Han, D.; Zhao, Y.-H.; Bai, S.-L. High-performance thermal interface materials consisting of vertically aligned graphene film and polymer. *Carbon* **2016**, *109*, 552–557. [[CrossRef](#)]
17. Wu, S.; Ladani, R.B.; Zhang, J.; Bafekrpour, E.; Ghorbani, K.; Mouritz, A.P.; Kinloch, A.J.; Wang, C.H. Aligning multilayer graphene flakes with an external electric field to improve multifunctional properties of epoxy nanocomposites. *Carbon* **2015**, *94*, 607–618. [[CrossRef](#)]
18. Zhu, X.; Mo, Z.; Zhang, C.; Wang, B.; Zhao, G.; Guo, R. Preparation of graphene-Fe<sub>3</sub>O<sub>4</sub> nanocomposites using Fe<sup>3+</sup> ion-containing magnetic ionic liquid. *Mater. Res. Bull.* **2014**, *59*, 223–226. [[CrossRef](#)]
19. Ma, E.; Li, J.; Zhao, N.; Liu, E.; He, C.; Shi, C. Preparation of reduced graphene oxide/Fe<sub>3</sub>O<sub>4</sub> nanocomposite and its microwave electromagnetic properties. *Mater. Lett.* **2013**, *91*, 209–212. [[CrossRef](#)]
20. Guo, L.; Xu, C.; Wang, X.; Lin, Y.; Li, Y.; Ji, W. Preparation of magnetic graphene. *Packag. Eng.* **2017**, 32–35.
21. Liu, Z.; Jiao, W.; Yan, M.; Li, J.; Ding, G.; Wang, R. A novel method for imitating nacre by utilizing magnetic graphene oxide and its magnetic field alignment in polymer nanocomposites. *Mater. Res. Express* **2018**, *5*. [[CrossRef](#)]
22. Renteria, J.; Legedza, S.; Salgado, R.; Balandin, M.P.; Ramirez, S.; Saadah, M.; Kargar, F.; Balandin, A.A. Magnetically-functionalized self-aligning graphene fillers for high-efficiency thermal management applications. *Mater. Des.* **2015**, *88*, 214–221. [[CrossRef](#)]
23. Wang, Y.; Zhao, Y.; Bao, T.; Li, X.; Su, Y.; Duan, Y. Preparation of Ni-reduced graphene oxide nanocomposites by Pd-activated electroless deposition and their magnetic properties. *Appl. Surf. Sci.* **2012**, *258*, 8603–8608. [[CrossRef](#)]
24. Mihai, A.I.; Garea, S.A.; Vasile, E.; Nistor, C.L.; Iovu, H. Functionalization of Porous Clay Heterostructures with Silane Coupling Agents. *Mater. Plast.* **2017**, *54*, 341–344. [[CrossRef](#)]
25. Ozgur, M.E.; Ulu, A.; Balcioglu, S.; Ozcan, I.; Koytepe, S.; Ates, B. The Toxicity Assessment of Iron Oxide (Fe<sub>3</sub>O<sub>4</sub>) Nanoparticles on Physical and Biochemical Quality of Rainbow Trout Spermatozoon. *Toxics* **2018**, *6*. [[CrossRef](#)]
26. Cao, R.; Fan, M.; Hu, J.; Ruan, W.; Xiong, K.; Wei, X. Optimizing Low-Concentration Mercury Removal from Aqueous Solutions by Reduced Graphene Oxide-Supported Fe<sub>3</sub>O<sub>4</sub> Composites with the Aid of an Artificial Neural Network and Genetic Algorithm. *Materials* **2017**, *10*. [[CrossRef](#)]

27. Chandra, V.; Park, J.; Chun, Y.; Lee, J.W.; Hwang, I.-C.; Kim, K.S. Water-Dispersible Magnetite-Reduced Graphene Oxide Composites for Arsenic Removal. *ACS Nano* **2010**, *4*, 3979–3986. [[CrossRef](#)]
28. Jiao, W.; Shioya, M.; Wang, R.; Yang, F.; Hao, L.; Niu, Y.; Liu, W.; Zheng, L.; Yuan, F.; Wan, L.; et al. Improving the gas barrier properties of Fe<sub>3</sub>O<sub>4</sub>/graphite nanoplatelet reinforced nanocomposites by a low magnetic field induced alignment. *Compos. Sci. Technol.* **2014**, *99*, 124–130. [[CrossRef](#)]
29. Si, Y.; Samulski, E.T. Synthesis of Water Soluble Graphene. *Nano Lett.* **2008**, *8*, 1679. [[CrossRef](#)]
30. Song, S.H.; Park, K.H.; Kim, B.H.; Choi, Y.W.; Jun, G.H.; Lee, D.J.; Kong, B.-S.; Paik, K.-W.; Jeon, S. Enhanced Thermal Conductivity of Epoxy Graphene Composites by Using Non-Oxidized Graphene Flakes with Non-Covalent Functionalization. *Adv. Mater.* **2013**, *25*, 732–737. [[CrossRef](#)]
31. Wan, Y.-J.; Li, G.; Yao, Y.-M.; Zeng, X.-L.; Zhu, P.-L.; Sun, R. Recent advances in polymer-based electronic packaging materials. *Compos. Commun.* **2020**, *19*, 154–167. [[CrossRef](#)]
32. Li, T.-L.; Hsu, S.L.-C. Enhanced Thermal Conductivity of Polyimide Films via a Hybrid of Micro- and Nano-Sized Boron Nitride. *J. Phys. Chem. B* **2010**, *114*, 6825–6829. [[CrossRef](#)] [[PubMed](#)]
33. Qin, L.; Li, G.; Hou, J.; Yu, X.; Ding, H.; Zhang, Q.; Wang, N.; Qu, X. Preparation, characterization, and thermal properties of poly (methyl methacrylate)/boron nitride composites by bulk polymerization. *Polym. Compos.* **2015**, *36*, 1675–1684. [[CrossRef](#)]
34. Hou, J.; Li, G.; Yang, N.; Qin, L.; Grami, M.E.; Zhang, Q.; Wang, N.; Qu, X. Preparation and characterization of surface modified boron nitride epoxy composites with enhanced thermal conductivity. *RSC Adv.* **2014**, *4*, 44282–44290. [[CrossRef](#)]